

Optical probing of spin dynamics of two-dimensional and bulk electrons in a GaAs/AlGaAs heterojunction system

This article has been downloaded from IOPscience. Please scroll down to see the full text article.

2010 New J. Phys. 12 113040

(<http://iopscience.iop.org/1367-2630/12/11/113040>)

View [the table of contents for this issue](#), or go to the [journal homepage](#) for more

Download details:

IP Address: 129.125.47.105

The article was downloaded on 19/11/2010 at 14:10

Please note that [terms and conditions apply](#).

Optical probing of spin dynamics of two-dimensional and bulk electrons in a GaAs/AlGaAs heterojunction system

P J Rizo¹, A Pugzlys^{1,3}, A Slachter¹, S Z Denega¹, D Reuter²,
A D Wieck², P H M van Loosdrecht¹ and C H van der Wal^{1,4}

¹ Zernike Institute for Advanced Materials, University of Groningen,
Nijenborgh 4, NL-9747AG Groningen, The Netherlands

² Angewandte Festkörperphysik, Ruhr-Universität Bochum,
D-44780 Bochum, Germany

E-mail: c.h.van.der.wal@rug.nl

New Journal of Physics **12** (2010) 113040 (21pp)

Received 1 June 2010

Published 19 November 2010

Online at <http://www.njp.org/>

doi:10.1088/1367-2630/12/11/113040

Abstract. The electron spin dynamics in a GaAs/AlGaAs heterojunction system containing a high-mobility two-dimensional electron gas (2DEG) have been studied in this paper by using pump-probe time-resolved Kerr rotation experiments. Owing to the complex layer structure of this material, the transient Kerr response contains information about electron spins in the 2DEG, an epilayer and the substrate. We analyzed the physics that underlies this Kerr response, and established the conditions under which it is possible to unravel the signatures of the various photo-induced spin populations. This was used to explore how the electron spin dynamics of the various populations depend on the temperature, magnetic field and pump-photon density. The results show that the D'Yakonov-Perel' mechanism for spin dephasing (by spin-orbit fields) plays a prominent role in both the 2DEG and bulk populations over a wide range of temperatures and magnetic fields. Our results are of importance for future studies on the 2DEG in this type of heterojunction system, which offers interesting possibilities for spin manipulation and control of spin relaxation via tunable spin-orbit effects.

³ Present address: Photonics Institute, Vienna University of Technology, Gusshausstrasse 27/387, 1040 Vienna, Austria.

⁴ Author to whom any correspondence should be addressed.

Contents

1. Introduction	2
2. Methods	3
2.1. Time-resolved probing of electron spins	3
2.2. Sample materials	6
2.3. Experimental setup	6
2.4. Relaxation processes and timescales	7
3. Results and discussion	8
3.1. Kerr signals from a GaAs/AlGaAs heterojunction system	8
3.2. Kerr signals from <i>i</i> -GaAs populations	14
3.3. Kerr signals from the two-dimensional electron gas population	17
4. Conclusions	19
Acknowledgments	20
References	20

1. Introduction

Spintronics is now a well-established field that aims to exploit the spin of electrons in addition to their charge [1]–[4]. The discovery of long spin dephasing times in bulk *n*-GaAs [5] prompted investigations of spin dynamics in several GaAs-based systems [6]. For double-sided quantum wells (QWs), various studies using optical techniques have aimed at understanding the more complex dynamics of two-dimensional (2D) electron spin ensembles [7]–[14]. Heterojunction systems, with a strongly asymmetric QW that contains a high-mobility 2D electron gas (2DEG), have also long attracted considerable interest. These systems provide the highest values for electron mobility. Further, this material is of interest since the QW asymmetry results in a strong and tunable Rashba spin–orbit coupling that can cancel the Dresselhaus spin–orbit coupling [15], and this gives access to control over spin relaxation and dephasing [14], [16]–[24]. However, most of what is known about electron spin dynamics in these heterostructures was obtained using transport measurements [15], [25]–[27]. Complementing this with optical pump–probe measurements allows for studies with ultrahigh time resolution.

We report here on using time-resolved magneto-optical Kerr rotation (TRKR) [28] for studying the dynamics of spin ensembles in such a heterojunction QW system that contains a high-mobility 2DEG. Initial TRKR studies on such systems suggest that this may also provide an interesting platform for studying electron–electron interactions [29, 30]. However, it is not yet well established in which regimes the Kerr response of 2DEG electrons can be reliably isolated from other contributions to the Kerr signal. The reason is that such multilayered GaAs/AlGaAs heterostructures have several GaAs layers that have optical transitions at nearly identical photon energies. This hinders discrimination of layers by tuning the laser photon energy when using very short pulses, and results in optical readout signals that contain contributions from (photo-excited) electron populations in several layers.

For our heterostructure, three different layers can contribute to the observed Kerr signals from electron spins: the 2DEG layer, the bulk epitaxial *i*-GaAs layer that forms the heterojunction and the *i*-GaAs substrate. We exploit that one can use differences in the *g*-factor

to isolate the signal from each population. The g -factor depends on the electron kinetic energy E (with respect to the bottom of the conduction band), which can be approximated as

$$g = g_0 + \gamma E, \quad (1)$$

where for bulk GaAs [31, 32] $g_0 \approx -0.44$ and $\gamma \approx 6.3 \text{ eV}^{-1}$. For 2DEG electrons these parameters were reported [32] as $g_0 \approx -0.377$ and $\gamma \approx 4.5 \text{ eV}^{-1}$. Due to band filling by (photo) electrons, the g -factor thus shifts with an increase of the (quasi-)Fermi level as well. A related consequence is that the g -factor shifts towards less negative values with increasing the degree of confinement in a QW (possibly with an increased shift from wavefunctions penetrating AlGaAs barriers). However, it is not obvious that discrimination by g -factors can be applied without accounting for electron momentum relaxation and the intermixing of the populations in different layers [33] during the evolution of spin dynamics. Our measurement technique relies on using a pump pulse that inserts optically oriented electron-spin populations well above the bottom of the conduction band, and subsequent momentum relaxation and diffusion of carriers can result in intractable Kerr signals. Nevertheless, our results show that one can define situations and regimes (defined by pump intensity) where the three spin populations can be studied without being hindered by these effects.

The g -factor of the 2DEG is well separated from that of the bulk layers, and our results show that the 2DEG population can be studied as an independent population when the density of photo-excited carriers does not exceed the 2DEG electron density from doping. The g -factor for the two bulk layers, on the other hand, is the same, so a different approach is needed to distinguish the signal originating from each. Here, we use the fact that our heterostructure contains a barrier that blocks carrier diffusion between the two bulk i -GaAs layers. The effect of this is that the carrier density in the layer closest to the surface reaches a higher average value. The effective g -factor for the uppermost i -GaAs layer then acquires a less negative value (equation (1)) than that of the underlying substrate. This can be applied in a regime where the density of photo-excited carriers exceeds the 2DEG electron density from doping, and under these conditions the signal from the 2DEG is suppressed by strong band filling in the 2DEG layer.

In section 2 of this paper, we discuss the experimental methods and sample materials. Results are presented in section 3. There, we first compare the Kerr response of our heterostructure to that of well-characterized [5, 34, 35] bulk n -GaAs material that is probed under identical conditions in our setup, and we highlight the differences. Next, we show that the response from the heterostructure can always be described as a superposition of signals from two independent electron populations, and we confirm that this is true both for the Kerr signals and for time-resolved reflectance signals that give us insights into carrier dynamics of the populations. Measurements of spin dynamics are then analyzed in both the time and frequency domains, confirming that it is possible to treat the different electron populations as independent. In order to confirm that we correctly assign each of the observed g -factors to a particular population in the heterostructure, we study how the g -factor, spin dephasing time and carrier lifetime of each population depend on pump-photon density and temperature.

2. Methods

2.1. Time-resolved probing of electron spins

Optical transitions across the bandgap in GaAs obey well-defined selection rules. This can be used for optical spin orientation: a circularly polarized laser pulse creates photo-excited

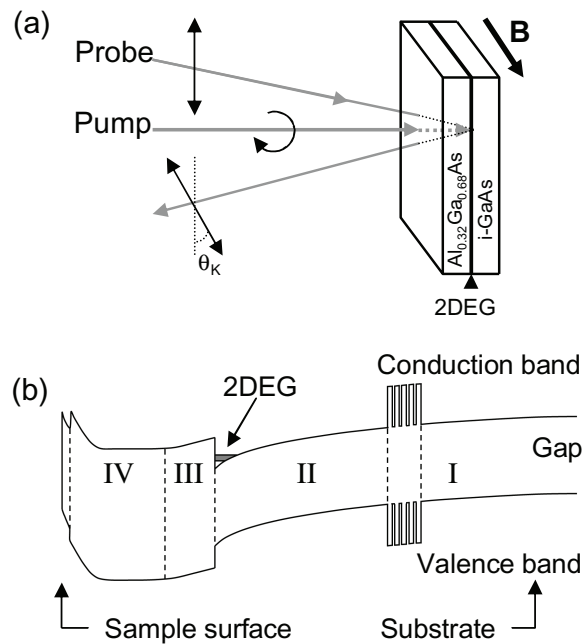


Figure 1. (a) Schematic diagram of the setup for TRKR measurements with pump and probe pulses incident on the 2DEG sample. The probe pulses are incident on the sample at a small angle from the normal ($\sim 2.3^\circ$). The applied magnetic field is oriented in the plane of the 2DEG. The rotation angle θ_K of the linear probe polarization is measured as a function of the time delay between pump and probe pulses. (b) Schematic diagram of the conduction and valence bands of the heterojunction system that contains a 2DEG (not to scale). The composition of layers I–IV is detailed in the main text.

electrons with a net spin polarization along the beam's direction [3, 36]. If the laser pulse is linearly polarized, there is no net spin orientation. In TRKR experiments, optical spin orientation with an ultrashort pump pulse is followed by optical spin probing with a weaker laser pulse with linear polarization that is reflected on the sample. An unequal filling of the spin-up and spin-down conduction bands gives rise to a transient difference in the absorption coefficient for right and left circularly polarized light (RCP and LCP). This also results in a difference in the refractive index for RCP and LCP light, and gives a rotation of the linear probe polarization upon reflection on an interface of the sample (given that the linear polarization is a superposition of RCP and LCP). This process is known as Kerr rotation, and the Kerr rotation angle θ_K (for probing with a certain photon energy) is proportional to the expectation value for spin orientation parallel to the propagation direction of the incident probe beam. The Kerr rotation is strongest when the probe photon energy is near resonance with transitions to the states with unequal spin filling, but its magnitude and sign depend on the detuning with respect to exact resonance [37, 38], and interference effects and additional Faraday rotations in systems with reflections from multiple interfaces [39]. Note that TRKR signals thus predominantly reflect the properties of electrons at the quasi-Fermi level of the photo-induced electron population. We studied the reflected probe with a polarization bridge with balanced photodetectors [28]. The recorded signal is then proportional to the Kerr rotation. Figure 1(a) depicts the experimental

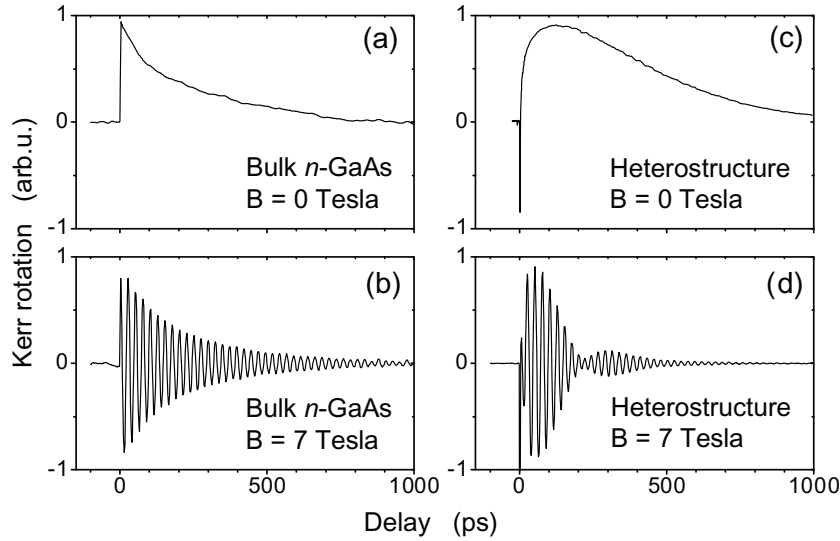


Figure 2. TRKR signal at 4.2 K from bulk n -GaAs at 0 tesla (a) and 7 tesla (b) and for the heterostructure containing a 2DEG, also at 0 tesla (c) and 7 tesla (d). The data show considerable differences between the spin signals from the bulk and 2DEG samples. Most remarkable is the presence of a node (at ~ 200 ps) in the Kerr oscillations measured at 7 tesla on the 2DEG sample (plot (d)). Comparing plots (a) and (c) also clearly shows a slow increase of the Kerr signal for the 2DEG sample for delays in the range 0–100 ps (also present in the 7 tesla data). Data taken with a photon density of $\sim 90 \times 10^{11}$ photons cm^{-2} per pump pulse.

setup. A TRKR trace is obtained by plotting the Kerr rotation angle θ_K as a function of the time delay between the pump and probe pulses (see for example figure 2).

In the presence of an in-plane external magnetic field (perpendicular to the initial orientation of the optically pumped spins), the injected spins precess around the field at the Larmor frequency ω_L ,

$$\omega_L = g\mu_B B/\hbar, \quad (2)$$

where g is the electron g -factor, μ_B is the Bohr magneton, B is the magnitude of the applied magnetic field and \hbar is the reduced Planck constant. In TRKR traces, this spin precession appears as oscillations of the Kerr angle at the Larmor frequency (figure 2(b)). Such traces can thus be used for determining the electron g -factor with equation (2).

We characterize the transient nature of TRKR traces with a Kerr signal decay time τ_K . Note that this can be shorter than the spin dephasing time T_2^* for an electron ensemble. We restrict the use of T_2^* to the case where the number of optically oriented electrons in the probe volume is constant. When this number is decreasing in time at a rate $1/\tau_e$ due to processes such as electron–hole recombination or diffusion out of the probe volume, the Kerr signal decays according to $1/\tau_K = 1/T_2^* + 1/\tau_e$ (an exception to this rule applies to electron doped systems, where Kerr signals can live longer than the recombination time [5]). We obtain τ_K from measuring TRKR traces at $B = 0$ or from studying the envelope of oscillatory signals at $B > 0$. In such TRKR traces, hole spins only contribute to the signal at very short pump–probe

delays (up to ~ 5 ps), because hole spins dephase very rapidly [40]–[44]. Thus, our TRKR measurements predominantly represent electron spin dynamics.

The dynamics of photo-excited carriers were studied independently of their spin polarization with time-resolved reflectance (ΔR) measurement. Here, a pump pulse with linearly polarized light is used. Subsequently, a collinearly polarized probe pulse is incident on the sample. The pump-induced changes in sample reflectance are measured by comparing the intensity of the reflected probe pulse in the presence and absence of a preceding pump pulse. This method thus probes the presence of pump-induced electrons and holes at energies that are resonant with the probe photon energy, as a function of pump–probe delay.

2.2. Sample materials

Figure 1(b) depicts the band profile of the heterostructure that we studied. Layer I is a (001)-oriented *i*-GaAs substrate. On this substrate a multilayer buffer consisting of ten periods of alternating GaAs (5.2 nm) and AlAs (10.6 nm) layers was grown. Layer II, the accumulation layer, consists of 933.0 nm of undoped GaAs. A spacer layer (III) is formed by 36.8 nm of undoped $\text{Al}_{0.32}\text{Ga}_{0.68}\text{As}$ grown on top of the accumulation layer. The donor layer (IV) consists of 71.9 nm of Si-doped $\text{Al}_{0.32}\text{Ga}_{0.68}\text{As}$ with $\sim 1 \times 10^{18}$ dopants cm^{-3} . The heterostructure is capped with 5.5 nm of *n*-GaAs. The two AlGaAs layers have a bandgap that is larger than all the photon energies that we used in our experiments. Due to quantum confinement the ~ 5 nm GaAs layers of the multilayer buffer and capping layer also only have optical transitions at energies above the photon energies that we use (and two-photon absorption processes for these layers can be neglected; an estimate based on the nonlinear coefficients for GaAs [45] shows that such processes contribute at our highest pump-photon density less than 1 part in 10^5 to the total absorption).

In this material, a 2DEG is formed at the heterojunction between layers II and III, in a QW with an effective width of ~ 15 nm (estimated with a numerical approach that is available at <http://www.nd.edu/~gsnider/>; [46]). Electron transport experiments on the 2DEG at 4.2 K, after illumination, gave $2.7 \times 10^6 \text{ cm}^{-2} \text{ Vs}^{-1}$ for electron mobility, and $4.7 \times 10^{11} \text{ cm}^{-2}$ for the electron density. We obtained nearly identical values with optical studies on our 2DEG material [47].

The bulk *n*-GaAs reference material had a doping concentration of $(2.4 \pm 0.2) \times 10^{16} \text{ cm}^{-3}$. Experiments on this material have shown that at this doping concentration very long spin dephasing times can be obtained with Kerr studies, and the dependence of spin dephasing times on various experimental conditions has been characterized [5, 34, 35].

2.3. Experimental setup

The measurement setup comprises a magneto-optical flow cryostat, pulsed laser, polarization optics and a detection system. Sample temperatures are varied between 4.2 and 100 K, and a superconducting magnet was used to apply fields up to 7 tesla. The magnetic field is set parallel to the plane of the sample while the laser pulses are incident normal to the sample plane as shown in figure 1(a). We used two different pulsed laser systems. Most of the results presented were obtained with a cavity-dumped mode-locked Ti : sapphire laser (further named laser 1) with 15 fs pulses corresponding to a fixed spectrum extending from 740 to 880 nm, and with repetition rates ranging from 4 to 80 MHz. This allows for wavelength tuning with

10 nm bandpass interference filters, and the central wavelength for the pump and probe beam can thus be chosen independently. After filtering, the pulse spectra have a significant amplitude in a 19 meV window. The filters are followed by prism compressors to ensure pulse durations with a full-width at half-maximum of approximately 120 fs at the sample. Unless stated otherwise, we present measurements from using laser 1 with the pump and probe pulse wavelengths centered at 780 and 820 nm, respectively. We reproduced most results in a setup with a tunable Ti : sapphire laser (further named laser 2) with ~ 150 fs pulses at 80 MHz repetition rate. The spectrum of pulses is wider than Fourier-transform limited, with significant amplitudes over a ~ 15 meV window. With this laser pump and probe, pulses were always centered at the same wavelength.

In each case, two beams derived from the laser are used as pump and probe with power ratio 24 : 1 or 4 : 1. We checked that all our results were at intensities below the regime where saturation effects occur: Kerr signals were always proportional to both the pump and the probe intensity, and the probe was always non-invasive in the sense that the observed decay times did not depend on probe intensity. We report the intensity of pump pulses in units of photons cm^{-2} per pulse, because it has relevance to the 2D electron density from doping. Note that this is the number of photons that are incident on the sample surface and that the number is smaller inside the sample due to reflection on each interface of the heterostructure. The pump–probe delay is varied with a retro-reflector on a translation stage. The two beams are focused on the sample with a 25 cm focal length spherical mirror, which gives spots with a diameter of approximately $150 \mu\text{m}$ full-width at base level.

To measure the transient Kerr rotation of the sample, a photo-elastic modulator (PEM) is used to modulate the polarization of the pump beam between RCP and LCP at a rate of 50 kHz. Besides improvement of signal-to-noise, this is crucial for avoiding dynamical nuclear polarization effects [35], and it rules out phase offsets in Kerr signals from interference effects in case of reflections from multiple interfaces [39]. The reflected probe is analyzed with a polarization bridge, which decomposes the probe beam into two orthogonal polarizations with a half-wave plate and a Wollaston prism, and which detects both these components with a pair of balanced photodetectors. This bridge is tuned to give a zero difference signal for probe pulses with zero Kerr rotation, and this difference signal is recorded with lock-in detection at the PEM frequency. For measurements with overlapping pump and pulse spectra, we employed a double modulation technique by adding an optical chopper in the probe beam (at $f_C \sim 1$ kHz) and recording a side band at f_C from the 50 kHz PEM frequency. In both cases, the signal is proportional to the Kerr rotation angle θ_K .

With this setup it is possible to measure transient reflectance (ΔR) and TRKR under identical conditions. For ΔR measurements the pump and probe beams have parallel linear polarizations. The reflected probe beam is now sent directly to a single photodetector, while the pump beam is modulated using an optical chopper. Modulations of the reflected probe intensity at the chopping frequency are then recorded with lock-in techniques. This gives a signal that is proportional to pump-induced reflectance change of the sample.

2.4. Relaxation processes and timescales

Before discussing the experimental data, it is useful to discuss a hierarchy of timescales that is relevant for interpreting our results. The electron spin dynamics occur at timescales of tens to hundreds of picoseconds, and the duration of the laser pulses thus have sufficient time resolution.

Hole spins dephase within ~ 5 ps [40]–[44]. Thus, the Kerr signal after a few picoseconds contains information about electron spins only.

The timescales of other electron and hole relaxation processes are very diverse, ranging from a few tens of femtoseconds to nanoseconds. We typically use a pump pulse with the photon energy centered at 780 nm, pumping electrons in GaAs layers at about 63 meV above the bottom of the conduction band. This leaves a non-equilibrium and non-thermal carrier distribution in the conduction and valence bands of the GaAs layers. Within the first hundreds of femtoseconds, electrons (and holes) thermalize into a Fermi–Dirac distribution with a carrier temperature that is much higher than the lattice temperature. Subsequently, electrons cool towards the lattice temperature. The initial momentum relaxation of electrons [48]–[53] with excess kinetic energy of more than 10 meV occurs very rapidly (within 10 ps). Once the excess kinetic energies drop below ~ 10 meV, further electron cooling slows down to a decay time of approximately 100 ps, depending on electron density. Note, however, that we use probe pulses with about 19 meV spectral width, with the probe spectrum centered at 820 nm, just below the bottom of the conduction band of GaAs. Consequently, most electrons relax into the spectral window of the probe within 10 ps, and the final cooling stage in the time interval from 10 to 100 ps has little influence on our Kerr and reflectance signals. Thus, the fast carrier thermalization and initial cooling allows for pumping the sample with high-energy photons (this also ensures that the penetration depth of pump light for the top GaAs layers is less than $1 \mu\text{m}$).

Right after a pump pulse, there will be a steep gradient in the photo-electron density along the direction of the pump over the length of the penetration depth. This equilibrates by electron diffusion. This takes place within the first 50 ps for high pump intensities, but may occur much more slowly [39] for low pump intensities. For our spot sizes, electron diffusion into directions perpendicular to the laser beam does not significantly change the electron density profile.

Other carrier processes that take place in timescales between 1 ps and 1 ns are exciton formation and carrier recombination. Within the first hundred picoseconds electrons and holes form excitons. This implies a further reduction of the initial energy of the photo-excited electrons by a few meV, but this occurs within the spectral window of our probe, and these processes do therefore not strongly influence our ΔR and TRKR traces. Electron–hole recombination, on the other hand, is directly visible in ΔR measurements. Obviously, recombination also results in loss of Kerr signal, especially in undoped samples or under conditions where the photo-excited electron density exceeds the electron density due to doping [28]. With time- and spectrally resolved photoluminescence, we measured that the exciton recombination time for our 2DEG sample at 4.2 K is greater than 2 ns in the accumulation layer, while it is approximately 360 ps for the substrate [47]. Both of these timescales become shorter with increasing pump intensity. As a function of temperature the 2DEG recombination time increases, while it decreases for bulk GaAs layers and n -GaAs.

3. Results and discussion

3.1. Kerr signals from a GaAs/AlGaAs heterojunction system

To highlight the Kerr response that is characteristic of the heterostructure, we compare it to Kerr measurements on the bulk n -GaAs sample that were obtained under identical conditions. Figure 2 shows in the left column TRKR signals from the bulk n -GaAs sample. Its Kerr signal at 0 Tesla closely resembles a mono-exponential decay. The signal at 7 tesla shows oscillations

at the Larmor precession frequency for electrons in GaAs (g -factor is $|g| \approx 0.44$ ^{Note 5}), with an envelope that again shows mono-exponential decay⁶. The transient TRKR signals from the heterostructure, on the other hand, are more complex. At 7 tesla (figure 2(d)), the Kerr response shows a node (at ~ 200 ps), indicating a beating between different precession frequencies. Additionally, the envelope shows a slow increase in the delay range from 0 to 100 ps, which is also observed at 0 tesla (figure 2(c)). The *in situ* comparison with bulk n -GaAs material is important for concluding that the observed beatings in TRKR traces are characteristic of the heterostructure, given that beatings can also appear in Kerr oscillations from n -GaAs under certain measurement conditions [35].

The heterostructure data in figures 2(c) and (d) also show a very sharp spike at very short delays, with a decay time of about 3 ps. It is also present in several other TRKR traces from the heterostructure that we will present and it was also observed with the n -GaAs sample at weaker pump intensities. It is longer than the duration of pump–probe overlap and therefore not an optically induced Stark effect [38] or the so-called coherent artifact [43]. Instead, it occurs during a timescale that is consistent with hole spin dephasing, and hot-carrier momentum relaxation (see section 2.4). The pump pulses also cause spin orientation of holes, and an unequal filling of different hole states will indeed also contribute to a signal for our balanced detection method. This part of the Kerr signal is therefore influenced by these effects, but full understanding goes beyond the scope of this paper. We further focus on the Kerr signals at delays of 5 ps and longer, and do not include this spike in further analysis.

Figures 3(a)–(c) show that the beatings and slow onset in the heterostructure Kerr signals appear for a wide range of pump intensities. However, the exact appearance clearly depends on pump intensity. In what follows we show that all three traces in figures 3(a)–(c) can be described as the superposition of two oscillatory signals with mono-exponential decay remarkably well. Each of the two contributions then results from a different electron population, each with its own decay time and effective g -factor. At the highest pump intensities (figure 3(a)), the signal is dominated by two bulk i -GaAs electron populations, one in the substrate (layer I in figure 1(b)) and the other in the accumulation layer (II). At the lowest pump intensity, (figure 3(c)) the signal is dominated by a population in the 2DEG QW and a second one with bulk i -GaAs characteristics.

Figure 3(d) shows the Fourier transform of the trace in figure 3(a). The amplitude spectrum shows two distinct peaks. It can be fitted very well with two Lorentzians, and the same holds for the Fourier transform of the traces in figures 3(b) and (c). This suggests that one can fit the traces in figures 3(a)–(c) in the time domain with a superposition of two mono-exponentially

⁵ For the n -GaAs sample and bulk populations in the heterostructure sample, we observe g -factors close to $|g| = 0.44$. At the highest pump intensities however, we observe values up to $|g| \approx 0.42$, as can be expected from band filling (see equation (1)). In addition, we observed for such high-pump-intensity traces that this effect diminishes over timescales of the electron–hole recombination times, resulting in weak g -factor drift during a TRKR trace that brings the g -factor back towards $|g| \approx 0.44$. We did not include this in our fitting as with equation (3), since it would give a much higher number of free parameters. However, this drift in g -factor values only gave small shifts ($< \pi$) in the phase of Kerr signals. We checked that the extracted τ_K values with our approach were not significantly different from fitting results where these effects were included.

⁶ The decay time of the Kerr signal for n -GaAs is in this measurement substantially shorter than the long values observed in other studies [5, 34, 35]. This is due to the high pump intensity and in exact agreement with the reported dependence on pump intensity [5]. With our setups we also observed Kerr signal decay times well in excess of 5 ns when using lower pump intensities and low fields.

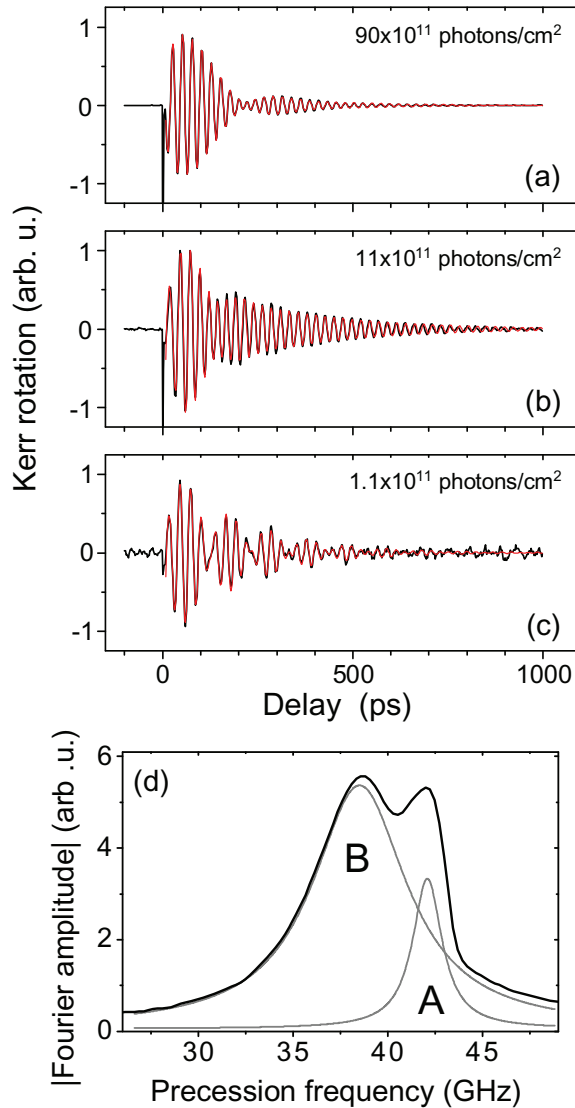


Figure 3. TRKR signal of the 2DEG sample for various pump-photon densities. The black traces in plots (a)–(c) show the experimental results at photon densities per pump pulse as labeled. The pump-photon density strongly influences the beating pattern in the Kerr oscillations. The red lines (on top of thicker black lines) show fits to the data using equation (3) (see main text for details). Plot (d) shows a Fourier transform (black line) of the TRKR data of plot (a), showing to distinct precession frequencies (with labels for populations A and B as in figure 5). Good fits to the spectrum can be obtained using a superposition of two Lorentzians (gray lines). Data taken at 7 tesla and 4.2 K.

decaying cosine functions. That also builds on observations in *n*-GaAs where TRKR signals from a single electron population with a single *g*-factor (see also figure 2(b)) can be described by a mono-exponentially decaying cosine function [5]. For this fitting we use

$$\theta_K = A_1 \exp\left(-\frac{t}{\tau_{K1}}\right) \cos(\omega_{L1}t + \phi_1) + A_2 \exp\left(-\frac{t}{\tau_{K2}}\right) \cos(\omega_{L2}t + \phi_2). \quad (3)$$

Here, t is the pump–probe delay, and τ_{K1} (τ_{K2}) and A_1 (A_2) are, respectively, the Kerr signal decay time and the Kerr rotation amplitude for each population. Similarly, ω_{L1} and ω_{L2} are the Larmor frequencies and ϕ_1 and ϕ_2 are apparent initial phases⁷ for spin precession. For fitting we only use data for $t > 5$ ps.

The fitting results from applying this to the experimental traces are presented as red traces in figures 3(a)–(c) (on top of the thicker black traces for the experimental results). The excellent fits demonstrate that the total signal can indeed be described as being composed of two distinct contributions from two different populations for $t > 5$ ps. We find that we can obtain very good fits assuming two populations only for all pump intensities. A similar approach that assumes three populations does not improve the fits significantly. This is a remarkable result, given that the Kerr response of our heterostructure does not necessarily split into two distinct contributions. The continuous character of the accumulation layer (II) from QW to bulk epilayer, followed by a bulk substrate, could give more complex signals with signatures of relaxation processes and mixing effects between populations [33]. We find that the sign of amplitudes A_1 and A_2 of the two contributions is always opposite (for ϕ_1 and ϕ_2 close to zero), which corresponds to Kerr rotations of opposite sign at $t = 0$. Consequently, the slow signal increase at early delays and the beatings in our Kerr oscillations have a common origin. The sign of the Kerr response depends on detuning from resonance, but we predominantly probe slightly red-detuned for all populations (the probe-photon energy was in most experiments a bit less than the bandgap). The opposite sign is therefore most likely from interference effects that play a role in the sign of Kerr response with reflections from multiple interfaces [39].

Further evidence that these excellent fits in the time domain indeed reflect that the physics that underlies our Kerr signals is that of two independent populations, each with a different but (nearly; see footnote 5) constant g -factor, comes from Fourier analysis of the traces. Scenarios that include significant spreads or strongly drifting g -factors due to momentum relaxation can be ruled out based on the phase spectrum of Fourier-transformed TRKR signals. In addition, direct measurements of the momentum-relaxation dynamics support this interpretation.

We applied time-resolved reflectance measurements for these studies of the momentum-relaxation dynamics. It provides a direct measure for the momentum relaxation of electron populations into the spectral window of the probe and subsequent electron–hole recombination. Figure 4 shows ΔR as a function of pump–probe delay measured on the heterostructure sample using different pump intensities. At high pump-photon densities, ΔR first reaches a negative peak before decaying back to zero. At low pump-photon densities, the signal first shows a positive ΔR , but at later delays ΔR obtains a negative value with only very slow decay back to zero.

We also find here that we can describe the full set of ΔR traces for $t > 10$ ps as the sum of two mono-exponentially decaying responses of opposite sign: one response with positive ΔR that is short lived and another response with negative ΔR that is long lived. In addition, for each trace during $0 < t \lesssim 10$ ps there is an onset proportional to $1 - \exp(-t/\tau_{mr})$, with a

⁷ We observe that using phases ϕ_i as free parameters is needed for obtaining good fits. We also observed this with the n -GaAs reference material (but not when pumping at low intensities close to the bottom of the conduction band). This is in contradiction to the expected direction of spin orientation parallel to the pump beam at $t = 0$. However, we only use data from delays $t > 5$ ps for fitting, since holes contribute to the Kerr signals up to $t \approx 5$ ps. For $t < 5$ ps, there is also rapid relaxation of electron kinetic energy E . Since the effective g -factor has a value closer to zero for higher E , early energy relaxation is consistent with apparent phase offsets for $t > 5$ ps. However, full justification of using ϕ_i as free parameters requires further investigation.

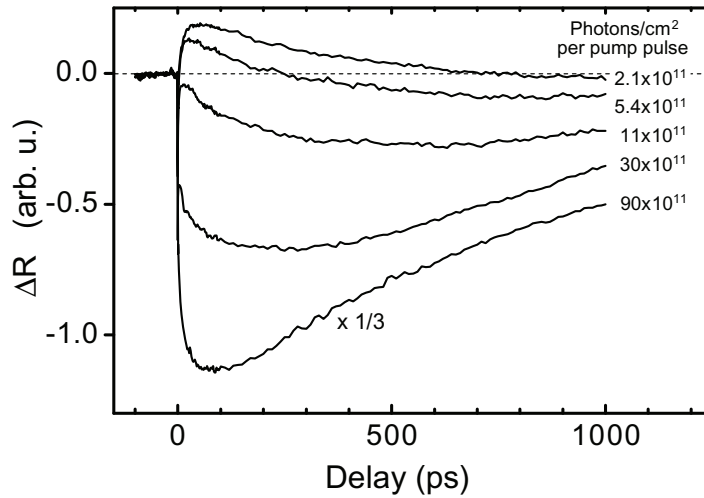


Figure 4. Transient reflectance (ΔR) traces from the 2DEG sample at different pump-photon densities. Data taken at 4.2 K and 0 Tesla.

decay $\tau_{\text{mr}} \lesssim 10$ ps. This is consistent with the initial momentum relaxation of pumped electrons into the spectral window of the probe. For $t > 10$ ps, we obtain excellent fits with an approach analogous to fitting TRKR signals with equation (3) (but with the cosine factors set to 1). The difference in shape for traces recorded at different pump intensities is then predominantly due to a shift in the relative weight of the two contributions.

At the lowest pump intensities, the signal is first dominated by a short-lived (~ 360 ps) positive contribution to ΔR . At later delays a longer-lived (2–3 ns) negative contribution dominates the signal. This is consistent with the photoluminescence results [47] if we assign the positive short-lived contribution to the substrate, and the negative long-lived contribution to the 2DEG layer. Going to higher pump intensities, the relative weight of the negative contribution (ratio $|A_2/A_1|$, with A_2 the amplitude of the negative contribution) increases from ~ 0.5 to ~ 5 . This is consistent with increased importance for the accumulation layer (II) that can be expected. In addition, the decay time for the negative long-lived population decreases to ~ 1 ns. Note, however, that at high pump intensity there is significant band-filling in the accumulation layer (II), so it should now be considered the recombination time for an electron population that is extended throughout this layer instead of a 2DEG population. At the high pump intensities, the onset of the strong negative contribution (with onset proportional to $1 - \exp(-t/\tau_{\text{mr}})$) curves over into the weak positive contribution with a decay time of $\lesssim 360$ ps, which makes it impossible to reliably fit this latter timescale for high pump intensities. When increasing the temperature to 100 K, the lifetime of the positive contribution gradually shortens to ~ 100 ps, while the lifetime of the negative contribution grows to ~ 8 ns.

Thus, we find that both TRKR signals and ΔR signals can be described very accurately as the superimposed response of two different electron populations. Moreover, the relative amplitudes A_1 and A_2 of populations that are observed with TRKR correlate with those observed in ΔR signals (further discussed at figure 5 below). The fact that the signal or signal envelope for each of the two contributions is well described by mono-exponential decay confirms that photo-excited electrons cool within about 10 ps to a temperature where all electrons are at energies within the spectral window of the probe. Further cooling only causes small changes in the

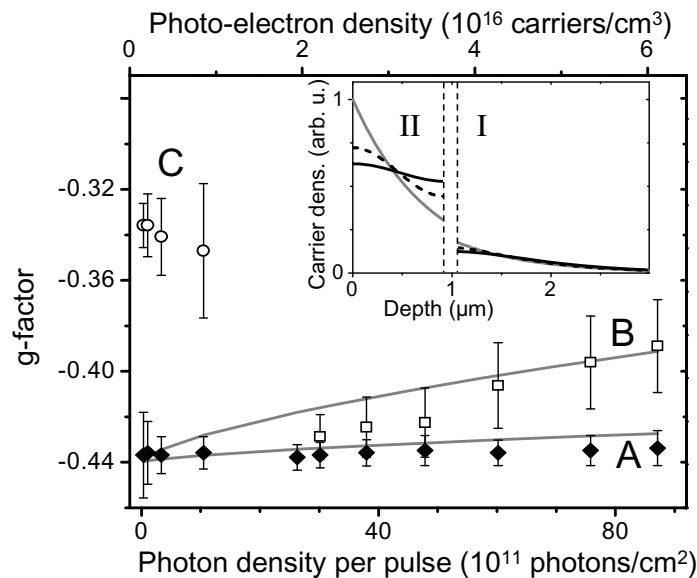


Figure 5. The g -factors of spin populations observed in the 2DEG sample as a function of pump-pulse photon density (bottom axis) and the estimated photo-excited electron density in the accumulation layer (top axis). At high photon densities two spin precession modes can be resolved with g -factors $|g| \approx 0.44$ (solid diamonds, population A) and $|g| \approx 0.39$ (open squares, population B). We ascribe these g -factors to electrons in the i -GaAs substrate (layer I) and electrons in the accumulation layer (layer II), respectively. The gray lines through the data points of A and B are calculated g -factor values (see main text for details). A third precession mode (open circles, population C) is observed at the lowest pump-photon densities and corresponds to electrons in the 2DEG. Data were obtained under the same conditions as in figure 3. The inset shows the calculated density of photo-excited electrons in the accumulation layer (layer II) and in the substrate (layer I) as a function of depth from the top of the accumulation layer. The dashed vertical lines at $0.933 \mu\text{m}$ show the position of the multilayer buffer. The gray line shows the calculated electron density immediately after photo-excitation with a 780 nm pump pulse. The dashed black line (solid black line) shows the electron density 20 ps (50 ps) after photo-excitation.

average value and spread of g -factors and are masked by the relatively short decay times of the Kerr signals. Further, we observe that for the substrate contribution to the signals, the decay times for the reflectance signals and Kerr signals are comparable. This means that the loss of Kerr signals is here for a significant part due to electron–hole recombination.

Although the TRKR traces from the heterostructure can always be fitted assuming two spin populations, a total of three different spin populations show up in the TRKR measurements when these are studied for a range of pump-pulse intensities. From such data, we analyze the precession frequencies of the different spin populations, both with Fourier analysis as in figure 3(d) and fitting in the time domain (equation (3)). Figure 5 shows which g -factors are observed as a function of pump-pulse intensity. The error bars indicate here the uncertainty in position for the two Lorentzian peak shapes that we fitted on the spectra and thus also give an

indication of the Kerr decay times for each contribution (the smallest error bars corresponding to ~ 250 ps and the largest to ~ 70 ps). Two spin populations show up at high pump-photon density (labeled A and B); a third population is only observed at low pump-photon density (labeled C). The ratio of contributions $|A_C/A_A|$, going over into $|A_B/A_A|$, increases from $\lesssim 1$ to ~ 5 with increasing pump intensity. It thus closely follows the ratio $|A_2/A_1|$ discussed for figure 4. This provides the first evidence that Kerr signal contributions B and C come from the accumulation layer, and A from the substrate. In the next sections (sections 3.2 and 3.3), we further discuss the origin of these three spin populations. We also analyze the physics that results in the fact that these populations behave independently, and the spin dynamics of each population.

3.2. Kerr signals from *i*-GaAs populations

The value of the g -factor of each population gives a strong indication of the medium that the electrons populate. The g -factors of the different semiconductor materials that make up the heterostructure are well known. The g -factor of electrons in bulk GaAs is approximately -0.44 [54], and electrons in heterojunction 2DEGs and 15–20 nm wide GaAs QWs have a g -factor of about -0.36 [12], [55]–[58]. For electrons in the 5.5 nm wide GaAs layers [59] $g \approx +0.15$, and for bulk $\text{Al}_{0.32}\text{Ga}_{0.68}\text{As}$ layers $g \approx +0.5$ [54] (but electron populations in the latter two layers are not interacting with the photon energies that we use).

The value of the g -factor of population A is $|g| \approx 0.44$ at all pump-photon densities. We therefore associate population A with electrons in bulk GaAs. Measurements of the temperature dependence of the g -factor of population A, discussed below, also indicate that these electrons populate a bulk layer of GaAs. TRKR measurements cannot directly determine the sign of g -factors. However, the g -factor of GaAs is known to be negative [54], so we assign a negative value to the g -factor of population A.

The g -factor of population B shows a strong dependence on pump-photon density. At the highest pump-photon densities the g -factor of population B is $|g| \approx 0.39$ (while the signal contribution B is here about five times stronger than A with its Kerr signal decay time as short as ~ 70 ps, see also the broad peak in figure 3(d)). As the photon density is reduced, the g -factor of population B approaches the value of $|g| \approx 0.44$. This shows that this population also corresponds to electrons in bulk GaAs, and we again assign a negative value to its g -factor. There are two bulk *i*-GaAs layers in the heterostructure: the accumulation layer (II, see figure 1) and the substrate (I). The analysis in the next paragraphs demonstrates that population A corresponds to electrons in layer I and that population B corresponds to electrons in layer II. Population C shows up in the TRKR measurements only at low pump-photon densities, and corresponds to 2DEG electrons, as will be further discussed in section 3.3.

At high pump-photon densities, the response from the two *i*-GaAs layers can be distinguished because different average electron densities are excited in each layer by the pump pulse, which results in different g -factors (equation (1)). In the following discussion, we show how different average electron densities are obtained thanks to a pump beam with short penetration depth and the multilayer buffer between layers I and II. At 4.2 K the absorption coefficient of 780 nm light in GaAs gives a penetration depth of approximately $0.77 \mu\text{m}$ [60]. The density of photo-excited electrons that is present immediately after a pump pulse decays exponentially as a function of depth into the GaAs layers over this length scale. Thus, most of the incident pump photons are absorbed in the accumulation layer (II), giving a much higher concentration of photo-excited electrons in this layer than in the substrate (I). The gray line

in the inset of figure 5 shows the density of photo-excited electrons as a function of depth immediately after the absorption of a pump pulse. This strong gradient in the photo-electron density will rapidly equilibrate due to diffusion. The inset also shows the calculated electron density as a function of depth 20 and 50 ps later. We used here a bulk diffusion constant [47, 61] of $30 \text{ cm}^{-2} \text{ s}^{-1}$, but the results of the model we present below are quite independent of the exact value of diffusion constant that is used. In this calculation, the influence of the space-charge potential on the accumulation layer is ignored. This is justified at high pump-photon densities because the space-charge potential is screened by the photo-excited carriers. In addition, carrier-recombination effects are ignored since these occur at timescales longer than the considered diffusion times. Note that the penetration depth for part of the probe spectrum (centered at 820 nm) is considerably longer than that of the pump, such that the Kerr response of the deepest photo-excited electrons is not strongly attenuated with respect to electrons near the surface. In addition, the reflection on the multilayer buffer layer ensures that there is an enhanced Kerr response for electrons in its direct vicinity.

The dashed vertical line in the inset of figure 5 at $0.933 \mu\text{m}$ represents the position of the multilayer buffer, which acts as a barrier that blocks electron diffusion. The calculated electron density profiles at 20 and 50 ps show that the electron density, and thus the quasi-Fermi level in the two layers, becomes discontinuous at the multilayer buffer. The accumulation layer reaches a much higher average electron density than the substrate (see also the top axis of figure 5 for estimated values), and thereby a much higher value for the quasi-Fermi level that is established after tens of picoseconds when most electrons are in the lowest available conduction band states (besides spin relaxation) due to cooling and diffusion. The average electron g -factor of a population that is observed in TRKR signals depends on the quasi-Fermi level as in equation (1). We used this to calculate the expected g -factors of electrons near the quasi-Fermi level for the population in the accumulation layer (II) and the substrate (I), without any adjustable parameters [40]. When calculating a photo-electron density from the pump-photon density that is incident on the heterostructure surface, we accounted for an estimate of the reflection on each interface in the heterostructure. These calculated g -factors are also plotted in figure 5. At high pump-photon density there is very good agreement between the measured and calculated g -factors for populations A and B (and also at low pump-photon density where A and B have the same g -factor). Around $40 \times 10^{11} \text{ photons cm}^{-2}$ the agreement is not as good. In this regime, the g -factors for A and B lie close together and it is here more difficult for the fitting procedure to distinguish two g -factors. Nevertheless, for almost all data points there is no significant disagreement between the simple model and the g -factors from fitting, and this provides a strong indication that the two populations are indeed electrons in the accumulation layer and the substrate.

The above discussion shows that the ability to distinguish the two populations relies on the short penetration depth for the pump pulse. Our results did not change significantly when using 800 nm pump and 820 nm probe photons (also showing that the initial rapid momentum relaxation does not result in significant spin dephasing). However, when using 820 nm photons for both pump and probe with laser 1, we did no longer observe the beatings in our TRKR oscillations. Under these conditions, the relative contribution from the population in the substrate is much higher due to deeper penetration of pump light into GaAs (the penetration depth increases beyond $3 \mu\text{m}$ when the wavelength increases beyond 820 nm [60]). This prohibits an analysis of the contribution to the Kerr signal from the top GaAs layers of the heterostructure. We could, nevertheless, fully reproduce our results in a mono-color experiment, explored with the tunable Laser 2. Also here, we had to ensure that the full spectrum of laser

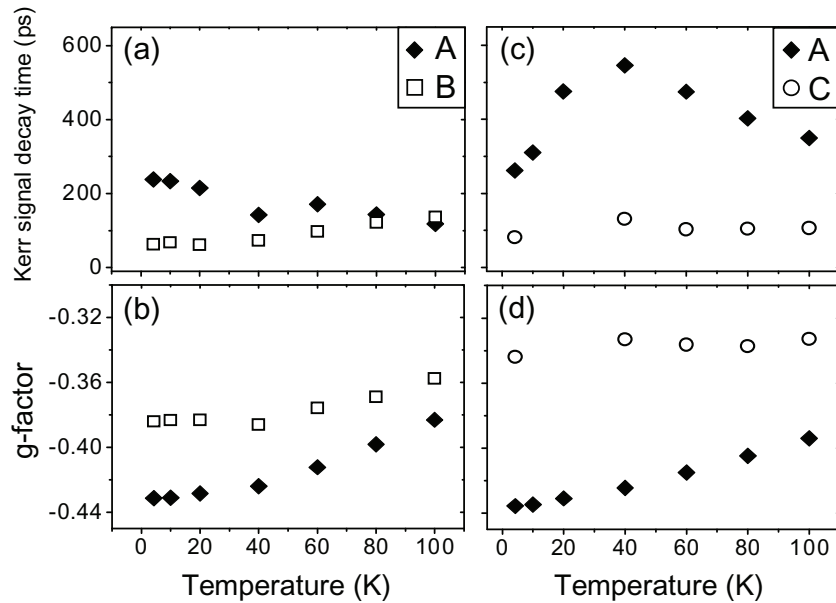


Figure 6. Kerr signal decay times (top row) and g -factors (bottom row) as a function of temperature, measured at pump photon densities of $\sim 100 \times 10^{11}$ photons cm^{-2} (left column) and $\sim 3.6 \times 10^{11}$ photons cm^{-2} (right column) in the heterostructure sample. Electron populations A, B and C (see also figure 5) are indicated by open squares, solid diamonds and open circles, respectively. The data points were obtained from fits with equation (3) to TRKR measurements taken at 7 tesla.

pulses had a short penetration depth. We could obtain results with a strong contribution from the accumulation layer to the Kerr response (both at high and low pump intensities) by setting the central laser wavelength at least ~ 20 meV above the bottom of the conduction band. Momentum relaxation brings electrons again rapidly near the bottom of the conduction band, and probing then occurs predominantly with the low-energy wing of our pulse spectrum. When tuning the central wavelength above ~ 810 nm, the Kerr response was again fully dominated by electrons in the substrate.

As an additional check for our interpretation in this regime with high pump-photon densities, we studied how the Kerr signals depend on temperature T (presented in figure 6) and magnetic field B (only discussed). The Kerr signal decay times for populations A and B as a function of temperature are presented in figure 6(a), and the corresponding g -factors in figure 6(b). These results were obtained from fitting equation (3) to TRKR measurements taken at $\sim 100 \times 10^{11}$ photons cm^{-2} per pump pulse. The temperature dependence of the g -factors of populations A and B is in agreement with observations by Oestreich *et al* [40] on GaAs bulk samples, confirming that populations A and B correspond to electrons with bulk GaAs characteristics. The g -factor of population B increases with temperature in a manner similar to population A. However, with increasing temperature the difference decreases. This is consistent with a broadening of the quasi-Fermi level with temperature, which increases the average electron kinetic energy E and (by equation (1)) brings the g -factor values closer to zero. At the highest temperatures, the broadening of the quasi-Fermi level starts to become larger than

the difference in quasi-Fermi level for populations A and B, which results in a smaller difference between the two g -factor values.

The Kerr signal decay times τ_{KA} and τ_{KB} of populations A and B show opposite trends as a function of temperature. Our analysis was that several mechanisms contribute to these Kerr signal decay times, and full understanding goes beyond the scope of this paper. Instead, we will only shortly summarize three mechanisms that contribute to the Kerr signal decay rates that we observe.

- (i) Electron–hole recombination. This directly contributes to loss of Kerr signals at the electron–hole recombination rate.
- (ii) Precessional dephasing due to a spread Δg in g -factor values. At high pump–photon densities, band-filling gives that the spin-oriented electrons have a spread in electron kinetic energy E , which (by equation (1)) directly results in a spread Δg . This results in a dephasing rate [5] $1/T_2^* = \Delta g \mu_B B / \sqrt{2}\hbar$. The magnetic field dependence of τ_{KA} and τ_{KB} showed that this mechanism gives a significant contribution at high fields.
- (iii) The D’Yakonov–Perel’ (DP) spin dephasing mechanism [63]–[65], as a result of the cubic Dresselhaus spin–orbit coupling in GaAs. The spins of electrons in motion experience a k -vector-dependent effective magnetic field. Consequently, random momentum scattering randomizes spin states by precession. We estimated the DP rates with a numerical Monte-Carlo approach [23].

In our experiments, these contributions are often of similar magnitude, but the weights shift with temperature, field and electron density in a manner that is consistent with our interpretation of the signal contributions A and B. A detailed account of this analysis can be found in [66].

3.3. Kerr signals from the two-dimensional electron gas population

Figure 5 shows that population C with $|g| \approx 0.34$ (besides a population with $|g| \approx 0.44$) can be observed when the pump-photon density drops below $\sim 10 \times 10^{11}$ photons cm^{-2} per pulse. This crossover occurs around the 2DEG electron density due to doping, and this provides another indication that population C resides in the 2DEG QW. We assume again that the g -factor of this population is negative, and its value (~ -0.34) is then indeed consistent with the g -factor of electrons in heterojunction 2DEG systems and 15–20 nm wide GaAs QWs [55, 57, 58]. Other electron populations that could be considered to give rise to the signal of population C can be convincingly rejected based on the g -factor values that we discussed earlier (section 3.2). One can also rule out that population C corresponds to electrons or excitons trapped at impurities or defects in bulk GaAs, since a g -factor of this value has not been observed before by us or by others in bulk GaAs samples.

We further remark that the g -factor values $|g| \approx 0.44$ and $|g| \approx 0.34$ rule out the interpretation that observing two populations at these low pump intensities results from simultaneous probing of electrons in two different subbands of the heterojunction QW. Electrons in excited subbands have a g -factor that is closer to zero than the g -factor $g \approx -0.34$ of electrons in the lowest subband [62]. Hence, the signal contribution with $|g| \approx 0.44$ cannot result from 2DEG electrons. Such an interpretation would also be inconsistent with the observed decay times for the two populations in both TRKR traces and ΔR traces. Instead, the population with $|g| \approx 0.44$ must be due to electrons with bulk GaAs characteristics around the multilayer buffer, and we label it again with A.

We carried out two additional experiments that confirm that population C corresponds to 2DEG electrons. In the first experiment, we performed TRKR measurements on a heterostructure where the 2DEG had been removed by wet etching to a depth of about 120 nm. On such material, one can still observe populations A and B at high pump-photon densities. At low pump-photon densities, however, population C is no longer observed, and Kerr signals only contain a contribution with $|g| \approx 0.44$. Secondly, we took TRKR data in an experiment where a microscope function was included in the setup with Laser 1, on a sample that had been processed into an ensemble of parallel wires of $1.2 \mu\text{m}$ width. This work showed that the signal contribution C was from electrons that can much more easily move along the wires than move to a neighboring wire (see [67] for further details).

At low excitation densities the spins of the 2DEG can thus be resolved. The second spin population visible under these conditions (labeled A, with $|g| \approx 0.44$) corresponds to electrons in a bulk GaAs layer. However, for these low pump intensities we were not able to determine whether the signal contribution A is dominated by electrons just above (in layer II) or below (in layer I) the multilayer buffer. Salis *et al* [39] recently reported that the drift of photo-electrons along the growth direction can be remarkably slow at low pump-photon densities, but for our system these effects are not yet fully understood. It is therefore difficult to determine whether all photo-electrons that are induced throughout the accumulation layer (II) rapidly drift into heterojunction QW (see figure 1(b)). We note, however, that the amplitude of signal contribution A is comparable to contribution C (unlike the strong-pumping regime, where A gives a ~ 5 times weaker contribution than B). This suggests that signal contribution A is from electrons in layer II, since a signal from electrons in the substrate (layer I) is expected to be much weaker than the signal contribution C due to multiple reflections (and probe absorption in the case of the mono-color experiment), and this is not observed.

In this regime with low pump-photon density, we could again only observe two populations when pumping well above the bottom of the conduction band for bulk GaAs. With the pump wavelength longer than 808 nm, the Kerr signals were dominated by a single population with $|g| \approx 0.44$. The population with $|g| \approx 0.34$ could be observed in both the two-color (laser 1) and mono-color (Laser 2) experiments when pumping with 808 nm or shorter pump wavelengths (see also the discussion in section 3.2). However, different from the case of the experiments at high pump-photon densities, it is now not only a matter of having a short penetration depth for the pump. Obtaining Kerr signals with a strong contribution from 2DEG electrons also profits from direct pumping into 2DEG subbands, and such transitions only obtain a significant matrix element when pumping at least ~ 20 meV above the bottom of the conduction band for bulk GaAs. This clearly must play a role when the drift of photo-electrons into the heterojunction QW is indeed a remarkably slow process at low pump intensities [39].

Also for this low pump-photon density regime we studied how the Kerr signals depend on temperature T (presented in figure 6) and magnetic field B . The Kerr signal decay times for populations A and C as a function of temperature are presented in figure 6(c), and the corresponding g -factors in figure 6(d), as obtained from fits with equation (3). The temperature dependence of the g -factor of population A follows again the trend that was reported for bulk GaAs [40], and agrees with the high pump-photon density results when accounting for the lower photo-electron density. The trend for C shows a weaker temperature dependence, in agreement with a weaker dependence on E for 2DEG electrons (equation (1)).

For the Kerr signal decay times (figure 6(c)), we obtained evidence that at 4.2 K the decay rate for both populations A and C is dominated by the DP spin dephasing mechanism, in

agreement with recent theory work [65]. We conclude this from experiments with large spots on 2DEG material that was etched into $1.2\ \mu\text{m}$ wide parallel wires. The decay times for both A and C then show a clear dependence on the crystal orientation of the wire [24]. This proves that the DP mechanism dominates, with spin–orbit fields that are highly anisotropic in k -space. For the 2DEG population (C), this conclusion agrees with earlier studies on high-mobility 2DEGs [8, 13, 15].

The Kerr signal decay times for population A are about 40 K longer than the electron–hole recombination times for bulk (as measured on bulk i -GaAs). This provides another indication that population A resides in a layer around the multilayer buffer where electron–hole recombination is suppressed due to band bending. The increase of the decay time for A when increasing the temperature up to 40 K indicates a suppression of the DP mechanism due to more rapid momentum scattering. Over the range of 40–100 K, the decay times shorten again. This agrees with recent theory work [65] that describes that the DP mechanism indeed dominates in this regime, at a rate that is limited by electron–electron scattering. Near 100 K, the thermal spread in electron kinetic energies E also becomes important, and results in a spread in g -factor values Δg that increases the precessional dephasing rate. A more detailed analysis can be found in [66].

4. Conclusions

We analyzed the physics that underlies the transient Kerr response of the 2DEG and epilayers of a GaAs/AlGaAs heterojunction system, and we characterized the dynamics of the various photo-induced spin ensembles in this material. This allowed us to establish the conditions under which it is possible to use ultrafast time-resolved Kerr rotation measurements for studying the spin dynamics of electron ensembles, and our results give insight into the possibilities and limitations of applying this method. The technique can be applied thanks to rapid momentum relaxation processes, which allow for pumping photo-electrons with an excess energy into the conduction band. At high pump-photon densities (above the 2DEG density from doping), this is crucial for having pump pulses with a short penetration depth, which ensures that Kerr detection is mainly probing electron populations in epilayers near the wafer surface. At low pump-photon densities, where 2DEG spins can be observed, the excess pump-photon energy is also needed for directly pumping into subbands of the 2DEG.

We studied with our TRKR method how the g -factors and spin dephasing times for the various populations depend on the temperature, magnetic field and pump-photon density. These results are consistent with theoretical work and similar results obtained with other experimental methods. The most interesting result here is that with low pump-photon density, the DP mechanism for spin dephasing (by spin–orbit fields) plays a prominent role in both the 2DEG and bulk populations at all our temperatures and magnetic fields. However, our analysis strongly indicates that several other mechanisms can contribute to the dephasing of spin-oriented electron populations and hence to the decay of Kerr signals. Complete understanding of these phenomena requires further studies, for which the results presented here provide a solid basis. It will be particularly interesting to apply our approach to further studies of the spin dynamics of 2D electron ensembles in systems where an electrostatic gate is added for tuning the asymmetric shape of the heterojunction QW. This yields a tunable Rashba spin–orbit coupling, which gives us access to a tunable suppression of spin dephasing and possibly even spin manipulation by spin–orbit fields [1, 3, 4].

Acknowledgments

We thank Bernard Wolfs, Ji Liu, Thorsten Last, Ka Shen and Ming-Wei Wu for help and useful suggestions and Bernd Beschoten for providing the bulk n -GaAs sample. This work was financially supported by the Dutch Foundation for Fundamental Research on Matter (FOM), the Netherlands Organisation for Scientific Research (NWO) and the German programs DFG-SFB 491, DFG-SPP 1285 and BMBF nanoQUIT.

References

- [1] Datta S and Das B 1990 *Appl. Phys. Lett.* **56** 665
- [2] Wolf S A, Awschalom D D, Buhrman R A, Daughton J M, von Molnár S, Roukes M L, Chtchelkanova A Y and Treger D M 2001 *Science* **294** 1488
- [3] Zutic I, Fabian J and Das S S 2004 *Rev. Mod. Phys.* **76** 323
- [4] Awschalom D and Samarth N 2009 *Physics* **2** 50
- [5] Kikkawa J M and Awschalom D D 1998 *Phys. Rev. Lett.* **80** 4313
- [6] Wu M W, Jiang J H and Weng M Q 2010 *Phys. Rep.* **493** 61
- [7] Ohno Y, Terauchi R, Adachi T, Matsukura F and Ohno H 1999 *Phys. Rev. Lett.* **83** 4196
- [8] Brand M A *et al* 2002 *Phys. Rev. Lett.* **89** 236601
- [9] Karimov O Z, John G H, Harley R T, Lau W H, Flatté M E, Henini M and Airey R 2003 *Phys. Rev. Lett.* **91** 246601
- [10] Averkiev N S *et al* 2006 *Phys. Rev. B* **74** 033305
- [11] Holleitner A W *et al* 2006 *Phys. Rev. Lett.* **97** 036805
- [12] Yugova I A *et al* 2007 *Phys. Rev. B* **75** 245302
- [13] Stich D *et al* 2007 *Phys. Rev. Lett.* **98** 176401
- [14] Koralek J D *et al* 2009 *Nature* **458** 610
- [15] Miller J B, Zumbühl D M, Marcus C M, Lyanda-Geller Y B, Goldhaber-Gordon D, Campman K and Gossard A C 2003 *Phys. Rev. Lett.* **90** 076807
- [16] Averkiev N S and Golub L E 1999 *Phys. Rev. B* **60** 15582
- [17] Schliemann J, Egues J C and Loss D 2003 *Phys. Rev. Lett.* **90** 146801
- [18] Bernevig B A, Orenstein J and Zhang S-C 2006 *Phys. Rev. Lett.* **97** 236601
- [19] Duckheim M and Loss D 2007 *Phys. Rev. B* **75** 201305
- [20] Cheng J L, Wu M W and da Cunha Lima I C 2007 *Phys. Rev. B* **75** 205328
- [21] Lü C, Schneider H C and Wu M W 2009 *J. Appl. Phys.* **106** 073703
- [22] Shen K and Wu M W 2009 *J. Supercond. Novel Magn.* **22** 715–7
- [23] Liu J *et al* 2010 *J. Supercond. Novel Magn.* **23** 11
- [24] Denega S Z *et al* 2010 *Phys. Rev. B* **81** 153302
- [25] Potok R M, Folk J A, Marcus C M and Umansky V 2002 *Phys. Rev. Lett.* **89** 266602
- [26] Koop E J, B J, van Wees Reuter D, Wieck A D and van der Wal C H 2008 *Phys. Rev. Lett.* **101** 056602
- [27] Frolov S M *et al* 2009 *Nature* **458** 868
- [28] Kikkawa J M, Smorchkova I P, Samarth N and Awschalom D D 1997 *Science* **277** 1284
- [29] Zhang F, Zheng H Z, Ji Y, Liu J and Li G R 2008 *Europhys. Lett.* **83** 47007
- [30] Ruan X Z, Luo H H, Ji Y, Xu Z Y and Umansky V 2008 *Phys. Rev. B* **77** 193307
- [31] Zawadzki W 1963 *Phys. Lett.* **4** 190
- [32] Yang M J, Wagner R J, Shanabrook B V, Waterman J R and Moore W J 1993 *Phys. Rev. B* **47** 6807
- [33] Malajovich I, Kikkawa J M, Awschalom D D, Berry J J and Samarth N 2000 *Phys. Rev. Lett.* **84** 1015
- [34] Hohage P E, Bacher G, Reuter D and Wieck A D 2006 *Appl. Phys. Lett.* **89** 231101
- [35] Schreiber L, Heidkamp M, Rohleder T, Beschoten B and Güntherodt G 2007 arXiv:0706.1884

- [36] D'yakonov M I and Perel' V I 1984 *Optical Orientation* ed F Meier and B P Zakharchenya (Amsterdam: Elsevier)
- [37] Lee Z K *et al* 1996 *Appl. Phys. Lett.* **69** 3731
- [38] Kimel A V *et al* 2001 *Phys. Rev. B* **63** 235201
- [39] Salis G and Alvarado S F 2006 *Phys. Rev. Lett.* **96** 177401
- [40] Oestreich M, Hallstein S, Heberle A P, Eberl K, Bauser E and Rühle W W 1996 *Phys. Rev. B* **53** 7911
- [41] Amand T, Marie X, Le Jeune P, Brousseau M, Robart D, Barrau J and Planel R 1997 *Phys. Rev. Lett.* **78** 1355
- [42] Linder N and Sham L J 1998 *Physica E* **2** 412
- [43] Hilton D J and Tang C L 2002 *Phys. Rev. Lett.* **89** 146601
- [44] Gerlovin I Ya *et al* 2004 *Phys. Rev. B* **69** 035329
- [45] Penzkofer A and Bugayev A A 1989 *Opt. Quantum Electron.* **21** 283
- [46] Tan I-H, Snider G L and Hu E L 1990 *J. Appl. Phys.* **68** 4071
- [47] Pugzlys A, Rizo P J, Ivanin K, Slachter A, Reuter D, Wieck A D, van der Wal C H and van Loosdrecht P H M 2007 *J. Phys.: Condens. Matter* **19** 295206
- [48] Leo K, Rühle W W and Ploog K 1988 *Phys. Rev. B* **38** 1947
- [49] Tatham M, Taylor R A, Ryan J F, Wang W I and Foxon C T 1988 *Solid-State Electron.* **31** 459
- [50] Kohl M, Freeman M R, Awschalom D D and Hong J M 1991 *Phys. Rev. B* **44** 5923
- [51] Rosenwaks Y, Hanna M C, Levi D H, Szymyd D M, Ahrenkiel R K and Nozik A J 1993 *Phys. Rev. B* **48** 14675
- [52] Alexandrou A, Berger V and Hulin D 1995 *Phys. Rev. B* **52** 4654
- [53] Yu P Y and Cardona M 2000 *Fundamentals of Semiconductors* (Berlin: Springer)
- [54] Weisbuch C and Hermann C 1977 *Phys. Rev. B* **15** 816
- [55] Snelling M J *et al* 1991 *Phys. Rev. B* **44** 11345
- [56] Snelling M J, Blackwood E, McDonagh C J, Harley R T and Foxon C T B 1992 *Phys. Rev. B* **45** 3922
- [57] Jiang H W and Yablonovitch E 2001 *Phys. Rev. B* **64** 041307
- [58] Meisels R 2005 *Semicond. Sci. Technol.* **20** R1
- [59] Hannak R M, Oestreich M, Heberle A P, Rühle W W and Köhler K 1995 *Solid State Commun.* **93** 313
- [60] Sturge M D 1962 *Phys. Rev.* **127** 768
- [61] Wolfe C M, Stillman G E and Lindley W T 1970 *J. Appl. Phys.* **41** 3088
- [62] Winkler R 2003 *Spin-Orbit Coupling Effects in Two-Dimensional Electron and Hole Systems* (Berlin: Springer)
- [63] D'yakonov M I and Perel' V I 1971 *Sov. Phys.—JETP* **33** 1053
- [64] D'yakonov M I and Kachorovskii V Yu 1986 *Sov. Phys.—Semicond.* **20** 110
- [65] Jiang J H and Wu M W 2009 *Phys. Rev. B* **79** 125206
- [66] Rizo P J 2010 *PhD Thesis* University of Groningen, Groningen, to be published
- [67] Rizo P J, Pugzlys A, Liu J, Reuter D, Wieck A D, van der Wal C H and van Loosdrecht P H M 2008 *Rev. Sci. Instrum.* **79** 123904